Synergistic Effect in Photocatalysis As Observed for Mixed-Phase Nanocrystalline Titania Processed via Sol–Gel Solvent Mixing and Calcination

ARTICLE *in* THE JOURNAL OF PHYSICAL CHEMISTRY C · JULY 2008

Impact Factor: 4.77 · DOI: 10.1021/jp712174y

Synergistic Effect in Photocatalysis As Observed for Mixed-Phase Nanocrystalline Titania Processed via Sol−Gel Solvent Mixing and Calcination

A. Zachariah, K. V. Baiju, S. Shukla,* K. S. Deepa, J. James, and K. G. K. Warrier

Ceramic Technology Department, Materials and Minerals Division (MMD). National Institute for Interdisciplinary Science and Technology (NIIST), (Formerly Regional Research Laboratory (RRL)), Council of Scientific and Industrial Research (CSIR) Industrial Estate P.O., Pappanamcode, Thiruvananthapuram, Kerala 695019, India

Received: December 31, 2007; Revised Manuscript Received: April 22, 2008

Mixed-phase nanocrystalline titania (TiO_2) with varying rutile content has been synthesized via solvent mixing and calcination (SMC) treatment of sol−gel-derived nanocrystalline anatase-TiO_2 and rutile-TiO_2 precursors. The mixed-phase nanocrystalline TiO_2 processed via sol−gel SMC has been characterized using X-ray diffraction, the scanning electron microscope, high-resolution transmission electron microscope, and ultraviolet−visible (UV−vis) diffuse reflectance spectroscope for analyzing its morphology, phase contents, nanocrystallite size distribution, and band gap. The photocatalytic activity of mixed-phase nanocrystalline TiO_2 processed via sol−gel SMC is measured by monitoring the degradation of the methylene blue dye in an aqueous solution, under the UV-radiation exposure, using the UV−vis absorption spectroscope. It is demonstrated that the photocatalytic activity of mixed-phase nanocrystalline TiO_2 processed via sol−gel SMC is a function of rutile content with the maximum photocatalytic activity observed for 40 wt% rutile. Thus, the synergistic effect has been observed between anatase-TiO_2 and rutile-TiO_2, which has been satisfactorily explained using a new model based on the band-gap variation in the connected nanocrystallites as a function of the size distribution and the phases involved, which overcomes the limitations of the existing models proposed earlier in the literature.

Introduction

Titania (TiO_2) is a well-known wide band-gap n-type semiconductor oxide used for the removal of highly toxic and nonbiodegradable pollutants present in air and wastewater via photocatalysis. The mechanism of photocatalysis involves adsorbing the pollutant molecules, from air or water, on the surface of TiO_2 particles, which are then excited using the ultraviolet (UV) radiation of the appropriate energy to generate electron (e^-) and hole (h^+) pairs within the particle volume. These e^-/h^+ pairs then migrate to the particle surface and serve as redox sites for the destruction of the surface-adsorbed pollutants.[1]

The photocatalytic activity of pure-TiO_2 has been known to be dependent on the various material parameters, which include the average nanocrystallite size, powder morphology, specific surface area, crystallinity, and phases involved.[2,3] Out of the two most popular phases of pure-TiO_2 (anatase and rutile), anatase-TiO_2 exhibits maximum photocatalytic activity. Interestingly, although rutile-TiO_2 shows lower photocatalytic activity, its addition in an optimum amount has been reported to enhance the photocatalytic activity of anatase-TiO_2 as a result of the synergistic effect between these two phases.[4–13]

Mixed-phase nanocrystalline TiO_2 with optimum rutile content has been usually obtained via high temperature calcination treatment of amorphous-TiO_2 or anatase-TiO_2,[7,9,11,12] changing the pH,[4] the anion concentration,[8] or the precursor[10] during the processing, and physical mixing of the precursors[4,8] In the present investigation, we synthesize mixed-phase nanocrystalline TiO_2 with varying rutile content via solvent mixing and calcination (SMC) treatment of anatase-TiO_2 and rutile-TiO_2 precursors derived using sol−gel. (Note*:* The 'SMC' is a newly coined term in this investigation, which involves the conventional physical mixing of the precursors followed by mixing in a solvent and subsequent drying and calcination treatments to remove the solvent for obtaining a dry mixed-phase powder with better electronic coupling between the phases involved). It is demonstrated here that mixed-phase nanocrystalline TiO_2 obtained via sol−gel SMC also exhibits optimum rutile content, corresponding to the maximum photocatalytic activity, which lies within the range reported in the literature. Such a systemic study showing the existence of optimum rutile content for mixed-phase nanocrystalline TiO_2 obtained via sol−gel SMC is presently not available in the literature.

Models based on the "charge-separation mechanism"[14] and the "antenna mechanism"[15] have been proposed earlier in the literature to explain the synergistic effect between the phases involved. However, none of these existing models can adequately explain the physical phenomenon responsible for the existence of optimum rutile content in mixed-phase nanocrystalline TiO_2 corresponding to the maximum photocatalytic activity. Hence, in this investigation, we propose a new model based on the band-gap variation in the connected nanocrystallites as a function of the size distribution and the phases involved. The present model satisfactorily predicts the existence of optimum rutile content, in mixed-phase nanocrystalline TiO_2, by overcoming the limitations of the earlier models.

Experimental Section

Chemicals. Titanium(IV) isopropoxide ($Ti[OC_3H_7]_4$) and anhydrous 2-propanol were purchased from Alfa Aesar, India, and methylene blue (MB) (AR grade) from Qualigens Fine Chemicals, India. All chemicals were used as received without any further purification.

* Corresponding author phone: +91-471-2515282; fax: +91-471-2491712; e-Mail: satyajit_shukla@csrrltrd.ren.nic.in.

10.1021/jp712174y CCC: $40.75
Published on Web 07/08/2008

Sol−Gel Processing of Nanocrystalline TiO_2. Nanocrystalline TiO_2 was synthesized via conventional sol−gel involving the hydrolysis and the condensation of $Ti[OC_3H_7]_4$ in an anhydrous alcohol.[2,16] For this purpose, a measured quantity of water was first mixed with 125 mL of anhydrous 2-propanol. A second solution was prepared in which 0.1 M (final concentration) of $Ti[OC_3H_7]_4$ was dissolved completely in 125 mL of anhydrous 2-propanol. Both solutions were sealed immediately and stirred rapidly using a magnetic stirrer to obtain homogeneous solutions. The solutions were prepared with the R (ratio of molar concentration of water to that of alkoxide precursor) value of 90. The water part of the solution was then added dropwise to the alkoxide part under continuous magnetic stirring. As a result of hydrolysis and condensation of $Ti[OC_3H_7]_4$ due to the reaction with water, the color of the solution changed from transparent to white. After the complete addition of the water part of the solution to that of the alkoxide part, the resulting solution was stirred overnight before drying in the furnace at 80 °C for the complete removal of the solvent and residual water. A part of the dried powder was then calcined at 400 °C for 1 h (termed here as "powder-A") to crystallize into anatase-TiO_2, and the remaining dried powder was calcined at 800 °C for 2 h (termed here as "powder-B") for crystallizing completely into rutile-TiO_2.

SMC Process for Producing Mixed-Phase Nanocrystalline TiO_2. Powder-A and powder-B processed via sol−gel were then utilized to obtain nanocomposites of anatase-TiO_2 and rutile-TiO_2, with different rutile content, via SMC. In the latter technique, powder-B was first mechanically mixed in different weight-ratios (0, 5, 10, 20, 40, 60, and 100 wt%) with powder-A. The mechanically mixed precursors were then dispersed in 100 mL of anhydrous 2-propanol under continuous magnetic stirring for 1 h to achieve homogeneous mixing. The suspension was then dried in an oven at 80 °C till the solvent was evaporated completely. The nanocrystalline TiO_2, with homogeneously mixed anatase-TiO_2 and rutile-TiO_2, was then calcined at 600 °C for 2 h for establishing an electronic coupling between the two mixed phases.

Characterization of Mixed-Phase Nanocrystalline TiO_2 Processed via Sol−Gel SMC. The crystalline phases present in the two precursors, powder-A and powder-B, as well as in mixed-phase nanocrystalline TiO_2 processed via sol−gel SMC were determined using X-ray diffraction (XRD, Rigaku, Japan). Broad-scan analysis was conducted within the 2θ range of 10−80° using the Cu Kα ($\lambda_{Cu} = 1.542$ Å) radiation. The obtained spectra were then utilized to determine the weight fraction of rutile-TiO_2 using the equation,

$$\text{rutile(wt\%)} = \frac{I_{(110)R} \times 100}{I_{(110)R} + (0.8)I_{(101)A}} \quad (1)$$

where, I_A and I_R represent the linear intensities of the main peaks of anatase-TiO_2 $(101)_A$ and rutile-TiO_2 $(110)_R$. Narrow-scan analysis was conducted within the 2θ range of 20−30° as the main peaks of anatase-TiO_2 and rutile-TiO_2 are contained within this range. These peaks were subsequently used to determine the average TiO_2 nanocrystallite size (D_{XRD}) using Scherrer's equation,

$$D_{XRD} = \frac{0.9\lambda}{\beta \cos \theta_B} \quad (2)$$

where D_{XRD} is the average nanocrystallite size (nm), λ the X-ray wavelength, β the full-width at the half-maximum intensity (in radian), and θ_B the half of the diffraction peak-angle ($2\theta_B$).

The morphology and the average aggregate size (D_{SEM}), in the two precursors and mixed-phase nanocrystalline TiO_2, were obtained using the scanning electron microscope (SEM, JEOL JSM-5600LV, Japan) operated at 15 kV.

Transmission electron microscope (TEM, Tecnai G^2, FEI, Netherlands) and high-resolution TEM (HRTEM) images of nanocrystalline TiO_2 powders processed under different conditions were obtained at 150−300 kV to study nanocrystallite size distribution. The selected-area electron diffraction (SAED) patterns were also obtained to confirm nanocrystallinity and the phases involved.

To determine the band gap of mixed-phase nanocrystalline TiO_2 with different rutile content, absorption spectra of the powders were obtained using the ultraviolet−visible (UV−vis) spectrophotometer (UV-2401 PC, Shimadzu, Japan) operated in the diffuse reflectance (DR) mode, for the wavelength within the range of 200−800 nm. The band gap was calculated using the equation,

$$\text{band} - \text{gap} = \frac{hc}{\lambda_{int}} \quad (3)$$

where, h is Plank's constant (4.135×10^{-15} eV·s), c the velocity of light (3×10^8 m·s^{-1}), and λ_{int} the wavelength (m) corresponding to the intersection of the extension of linear part of the spectrum and the x-axis.

Photocatalytic Activity of Mixed-Phase Nanocrystalline TiO_2 Processed via Sol−Gel SMC. The photocatalytic activity of the sol−gel-derived precursors and mixed-phase nanocrystalline TiO_2 processed via sol−gel SMC was studied by monitoring the degradation of the MB dye in an aqueous suspension containing nanocrystalline TiO_2 under UV-radiation exposure with continuous magnetic stirring. A 75 mL of aqueous suspension was prepared by completely dissolving 0.0064 μmol·L^{-1} of the MB dye and then dispersing 0.4 g·L^{-1} of nanocrystalline TiO_2 in the deionized water. The resulting suspension was equilibrated by stirring in the dark (without the UV-radiation exposure) for 1 h to stabilize the adsorption of the MB dye over the surface of nanocrystalline TiO_2.

The stable aqueous suspension was then exposed to the UV radiation, with continuous magnetic stirring, using the Rayonet Photoreactor (The Netherlands) containing 15 W tubes (Philips G15 T8) as the UV source, which emitted UV radiation having a wavelength within the range of 200−400 nm (corresponding to a photon energy range of 3.07−6.14 eV). Following UV-radiation exposure, 3 mL of aqueous suspension was taken out of the UV chamber after each 10 min interval for a total 1 h of UV-radiation exposure for obtaining the absorption spectrum.

Nanocrystalline TiO_2 was separated from the sample suspension using a centrifuge (R23, Remi Instruments India Ltd.), and the supernatant was examined using a UV−vis spectrophotometer to study the degradation of the MB dye. The absorption spectra of the MB dye solution were obtained within the range of 200−800 nm as a function of the UV-radiation exposure time for the two precursors and mixed-phase nanocrystalline TiO_2 with different rutile content. The intensity of the main absorption peak (A) of the MB dye solution, located at 656 nm, was taken as a measure of the residual MB dye concentration (C). The UV−vis absorption spectrum of the MB dye solution, without the addition of nanocrystalline TiO_2 and the UV-radiation exposure, was also recorded as a reference spectrum corresponding to the initial MB dye concentration (C_0). The normalized residual MB dye concentration was calculated using the relationship of the form,

$$\left(\frac{C}{C_0}\right)_{MB} = \left(\frac{A_{time=t}}{A_{time=0}}\right)_{656nm} \quad (4)$$

A photocatalysis experiment was also performed in the absence of nanocrystalline TiO_2 photocatalyst to confirm the stability of the MB dye in an aqueous solution under continuous UV-radiation exposure. Under this condition, the initial MB dye concentration (C_0) remained unchanged even after sample irradiation for a total of 1.5 h.

Results

Structural Analysis of Mixed-Phase Nanocrystalline TiO_2 Processed via Sol−Gel SMC. Broad-scan XRD spectra obtained using the precursors, powder-A and powder-B, are presented in Figures 1a and 1b. It is seen that powder-A is primarily anatase-TiO_2 (97 wt%, as determined using eq 1) with the D_{XRD} of ~10 nm (as determined using eq 2), while powder-B is primarily rutile-TiO_2 (90 wt%, as determined using eq 1) with the D_{XRD} of ~40 nm (as determined using eq 2). The phases are identified by comparing the spectra with the JCPDS files # 21-1272 and # 21-1276. During the sol−gel SMC, it was assumed that powder-A and powder-B consist of only anatase-TiO_2 and rutile-TiO_2, respectively. However, broad-scan XRD analysis suggests that they contain a small amount of rutile-TiO_2 and anatase-TiO_2 in their structures.

Typical broad-scan XRD spectra obtained using mixed-phase nanocrystalline TiO_2 with rutile content of 10, 20, and 40 wt% (based on the synthesis conditions) are presented in Figures 2a−c, respectively. It is clearly seen that with increasing addition of rutile-TiO_2 during the sol−gel SMC, the intensity of the main rutile peak in the XRD spectra also increases. Using eq 1, the weight fractions of rutile-TiO_2 in Figures 2a−c are calculated to be 13, 25, and 37 wt%, respectively, which are comparable with those considered during the processing of mixed-phase nanocrystalline TiO_2. As determined using eq 2, the D_{XRD} of anatase-TiO_2 is estimated to be 24, 27, and 29 nm, respectively, while that of rutile-TiO_2 is estimated to be 30, 60, and 47 nm, respectively. (Note: In this manuscript, unless otherwise stated, the amount of rutile (wt%) corresponds to that considered during the processing of mixed-phase nanocrystalline TiO_2 via sol−gel SMC.)

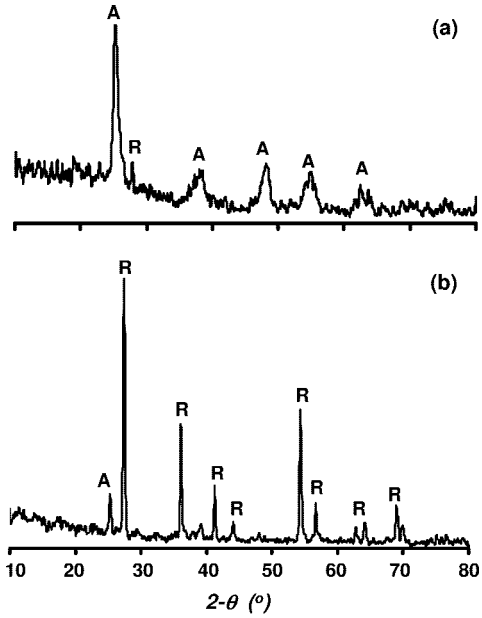

Figure 1. Broad-scan XRD spectra obtained for the two sol−gel-derived precursors, powder-A (a) and powder-B (b). A and R represent diffraction peaks corresponding to anatase-TiO_2 and rutile-TiO_2, respectively.

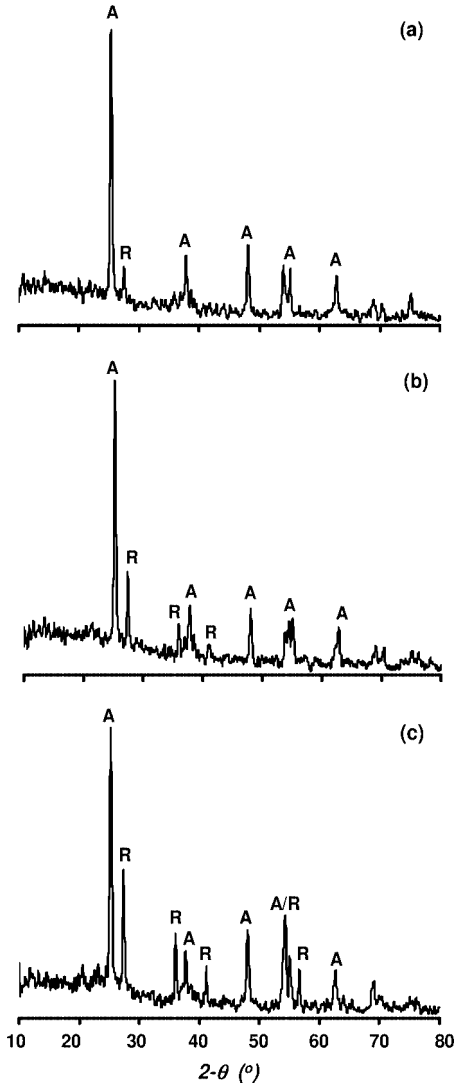

Figure 2. Broad-scan XRD spectra obtained for mixed-phase nanocrystalline TiO_2 processed via sol−gel SMC with rutile content of 10 (a), 20 (b), and 40 (c) wt%. A and R represent diffraction peaks corresponding to anatase-TiO_2 and rutile-TiO_2, respectively.

Morphology of Mixed-Phase Nanocrystalline TiO_2 Processed via Sol−Gel SMC. The SEM micrographs of nanocrystalline TiO_2 powders processed under different conditions are presented in Figure 3. Powder-A, which is calcined at 400 °C for 1 h, Figure 3a, appears to consist of small-size particles (D_{SEM} ~ 100−150 nm) of anatase-TiO_2 with minimum aggregation. However in Figure 3b, powder-B, which is calcined at 800 °C for 2 h, is seen to consist of highly aggregated relatively large-size particles (D_{SEM} ~ 300 nm) of rutile-TiO_2. Typical morphology of mixed-phase nanocrystalline TiO_2 processed via sol−gel SMC with 40 wt% rutile, Figure 3c, appears to be a mixture of the morphologies observed in Figures 3a and 3b.

Nanocrystallite Size Distribution in Mixed-Phase TiO_2 Processed via Sol−Gel SMC. TEM and HRTEM images obtained using nanocrystalline TiO_2 processed under different conditions are presented in Figures 4−6. In Figure 4, TEM images obtained using the precursor powder-A are presented at different magnifications. Figure 4a shows near-spherical-

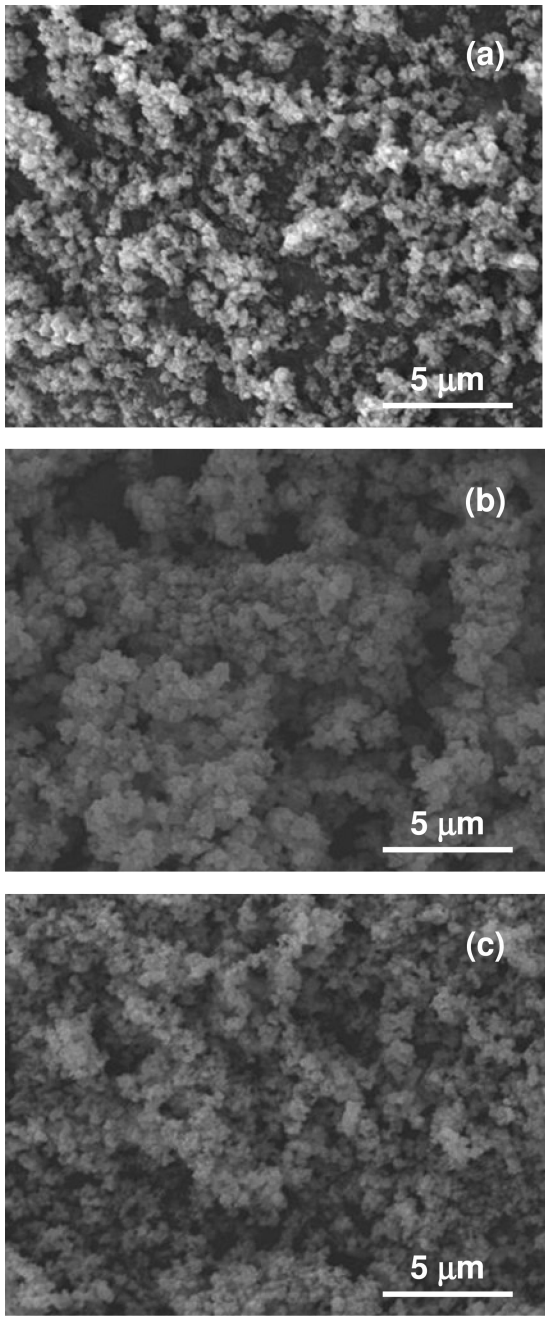

Figure 3. SEM micrographs of the sol−gel-derived precursors, powder-A (a) and powder-B (b), and mixed-phase nanocrystalline TiO_2 with optimum rutile content of 40 wt% processed via sol−gel SMC (c).

shaped aggregates with the average size of ∼100 nm, which are agglomerated to form a single large-size particle. These aggregates are further noted to consist of small nanocrystallites. The SAED pattern obtained using this large-size particle, shown as an inset in Figure 4a, displays continuous rings suggesting both the small size of nanocrystallites within the aggregates and their crystalline nature. In Figure 4b, the HRTEM image of one of the aggregates is shown, which reveals the presence of nanocrystallites of different sizes less than 10 nm. The aggregate appears to be porous with the pore size in the mesoporous range. The HRTEM images of two near-spherical nanocrystallites of size ∼4 nm and ∼10 nm, having different lattice orientations, are presented in Figure 4c.

In Figure 5, the TEM image obtained using the precursor powder-B is presented. Nanocrystallites of size ∼100−150 nm

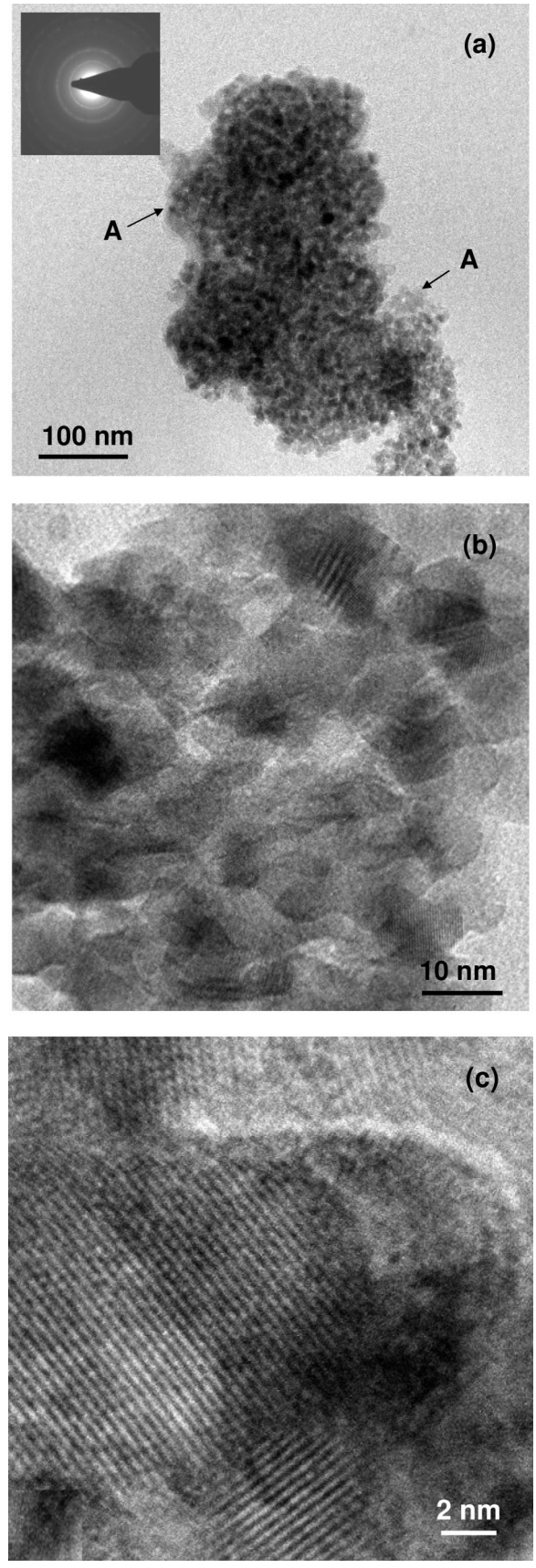

Figure 4. TEM (a) and HRTEM (b, c) images of the sol−gel-derived precursor, powder-A, obtained at different magnifications. The inset in part a shows the corresponding SAED pattern. A represents anatase-TiO_2.

are observed to form aggregates of size ∼300−500 nm, which in turn form a porous agglomerate. The SAED pattern as shown

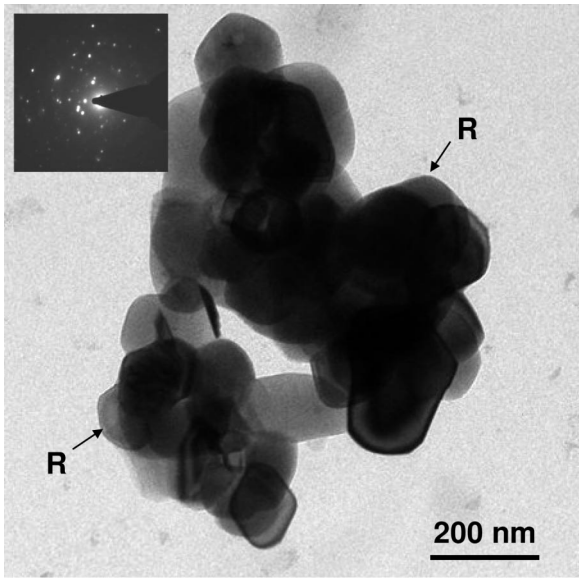

Figure 5. TEM image of the sol−gel-derived precursor, powder-B. The inset shows the corresponding SAED pattern. R represents rutile-TiO_2.

in the inset is seen to be spotty, revealing both the large size of nanocrystallites and their crystalline nature. Comparison with Figure 4 shows that nanocrystallites of rutile-TiO_2 are much coarser than those of anatase-TiO_2. Further comparison shows that nanocrystallites of rutile-TiO_2 and their aggregates have morphologies which are distinct relative to those of nanocrystallites of anatase-TiO_2 and their aggregates. Nanocrystallites of rutile-TiO_2 are more faceted, Figure 5, than those of anatase-TiO_2, Figure 4c.

The TEM and HRTEM images, obtained using the mixed-phase nanocrystalline TiO_2 with 40 wt% rutile, are presented in Figure 6. In Figure 6a, an aggregate of TiO_2 nanocrystallites of size ∼2 μm is seen. The morphology of the powder suggests that the aggregate contains nanocrystallites of both anatase-TiO_2 and rutile-TiO_2 as marked A and R in Figure 6a, which is in consonance with the morphology observed in the SEM micrograph presented in Figure 3c. The corresponding SAED pattern is shown as an inset in Figure 6a, which reveals both the continuous ring pattern as well as the spotty pattern. This also suggests that the powder contains both anatase-TiO_2 and rutile-TiO_2. At higher magnification, Figure 6b, the interface between the aggregated nanocrystallites of anatase-TiO_2 of size ∼20−25 nm and one of the large-size (∼150 nm) nanocrystallites of rutile-TiO_2 could be revealed, which suggests strong electronic interaction between the two phases. As shown in Figures 6c and 6d, nanocrystallites forming the isolated aggregates of anatase-TiO_2 (marked as A) and rutile-TiO_2 (marked as R), which are not in physical contact with each other, were also detected. In Figure 6c, the size of nanocrystallites of anatase-TiO_2 is noted to be ∼25−35 nm, which is comparable with that (∼29 nm) estimated using the XRD. However, in Figure 6d, the size of nanocrystallites of rutile-TiO_2 is observed to be ∼150−200 nm, which is much larger than that (∼47 nm) estimated using the XRD. (Note: This discrepancy in the size of nanocrystallites of rutile-TiO_2, estimated using the two different techniques, can only be explained if it is assumed that nanocrystallites of rutile-TiO_2, Figure 6d, contain subgrains of smaller size).

Band-Gap Determination for Mixed-Phase Nanocrystalline TiO_2 Processed via Sol−Gel SMC. UV−vis DR absorption spectra of mixed-phase nanocrystalline TiO_2, containing different amounts of rutile, are presented in Figure 7. For mixed-phase nanocrystalline TiO_2 containing primarily anatase-TiO_2, a significant increase in the absorbance is seen below 385 nm, which corresponds to the band gap of 3.3 eV as calculated using eq 3. With an increasing amount of rutile from 0 to 40 wt%, the absorbance for the wavelengths above 385 nm is noted to increase. As shown in the inset, a systematic red shift in the absorbance spectra with increasing rutile content is clearly seen. For mixed-phase nanocrystalline TiO_2 with 60 wt% rutile, the shift in the absorbance above 385 nm is distinctly noticeable with the calculated band-gap value of 3.02 eV.

Photocatalytic Activity of Mixed-Phase Nanocrystalline TiO_2 Processed via Sol−Gel SMC. Typical variation in the normalized residual MB dye concentration as a function of UV-radiation exposure time, as obtained using eq 4, for the two precursors (powder-A and powder-B) and mixed-phase nanocrystalline TiO_2 with rutile content of 0, 10, and 40 wt%, are presented in Figure 8a. It is observed that the kinetics of the photocatalytic activity, measured in terms of the degradation of the MB dye, is much slower for the two sol−gel-derived precursors. However, after the SMC process, the addition of rutile-TiO_2 to anatase-TiO_2, with the strong electronic interaction in between them, results in an improvement in the kinetics of the photocatalytic activity of mixed-phase nanocrystalline TiO_2.

Typical plots for determining the apparent first-order reaction-rate constant (k_{app}), obtained using the data presented in Figure 8a, are shown in Figure 8b. The k_{app} values for the mixed-phase nanocrystalline TiO_2, having different amounts of rutile, are obtained from the slopes of these fitted straight lines.

The variation in the k_{app} (obtained using the graphs similar to those shown in Figure 8b) and that in the normalized residual MB dye concentration corresponding to 60 min of UV-radiation exposure (obtained using the graphs similar to those shown in Figure 8a) as a function of amount of rutile, are presented in Figure 9. In Figure 9a, the k_{app} is noted to increase first with increasing amount of rutile within the range of 0−40 wt%. The k_{app} reaches the maximum value for 40 wt% rutile, beyond which it is seen to decrease with further increase in rutile content. The dotted line joining the k_{app} values of pure anatase-TiO_2 and pure rutile-TiO_2 represents the hypothetical path which would be followed in the absence of strong electronic interaction between the phases involved.

In Figure 9b, the normalized residual MB dye concentration, corresponding to 60 min of UV-radiation exposure, is seen to decrease first with the addition of rutile-TiO_2 to anatase-TiO_2. Similar to the observation made in Figure 9a, the minimum residual MB dye concentration is noted for 40 wt% rutile, beyond which it increases with further increase in the rutile content. Again, the dotted line joining the normalized residual MB dye concentration values of pure anatase-TiO_2 and pure rutile-TiO_2 represents the hypothetical path which would be followed in the absence of strong electronic interaction between the phases involved. Thus, the experimentally observed variation in both the k_{app} and the normalized residual MB dye concentration as a function of the amount of rutile, in the mixed-phase nanocrystalline TiO_2, reveals a drastic change in the slopes of the graphs relative to those of the dotted lines, when rutile content increases from 0 to 40 wt%. This strongly suggests the existence of the synergistic effect between anatase-TiO_2 and rutile-TiO_2 in the mixed-phase nanocrystalline TiO_2 processed via sol−gel SMC.

Discussion

In the present investigation, the two precursors, powder-A, which is primarily anatase-TiO_2, and powder-B, which is

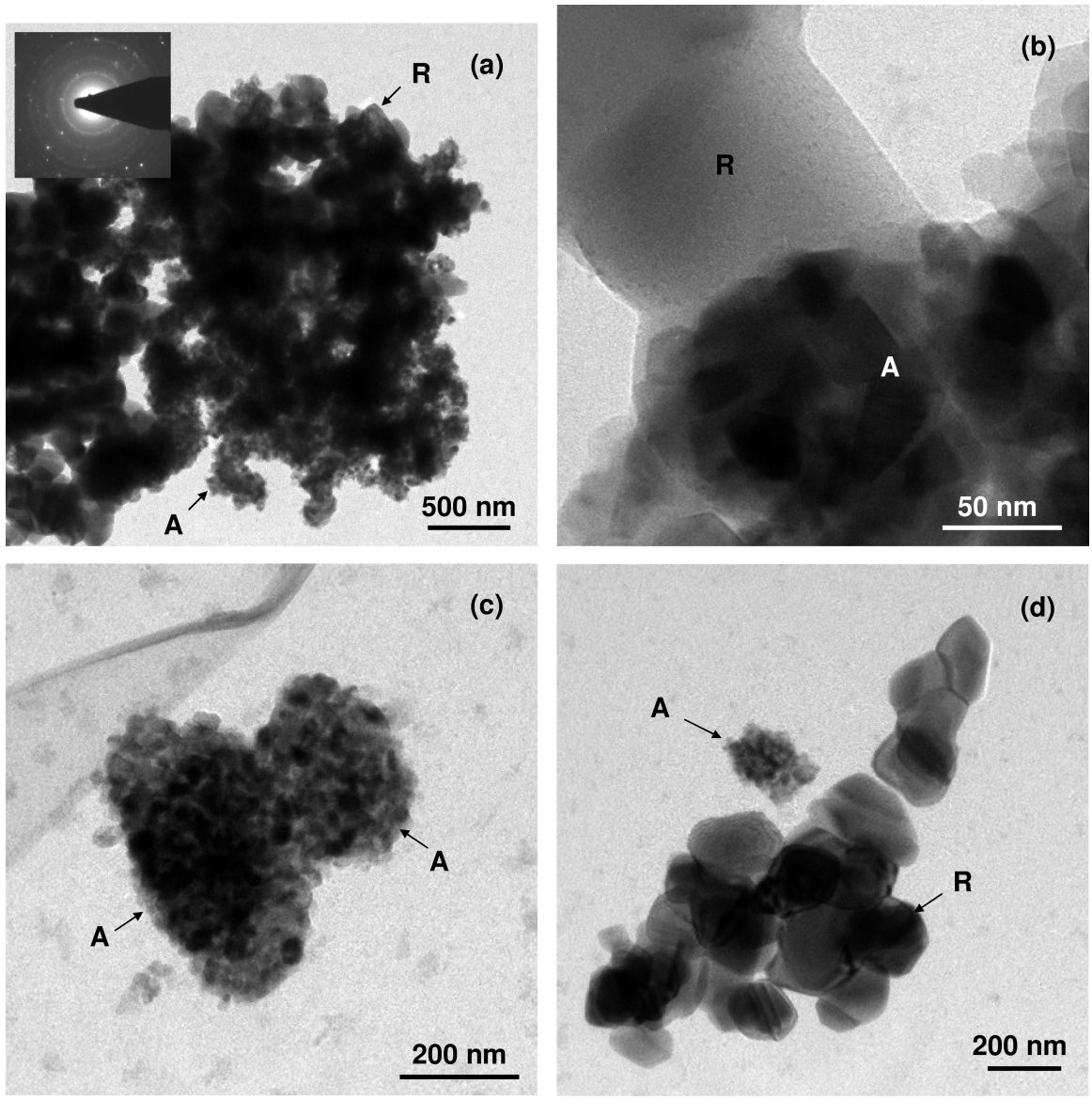

Figure 6. TEM images of mixed-phase nanocrystalline TiO_2, with an optimum rutile content of 40 wt%, processed via sol−gel SMC. The images are obtained at different magnifications. The inset in part a shows the corresponding SAED pattern. A and R represent anatase-TiO_2 and rutile-TiO_2.

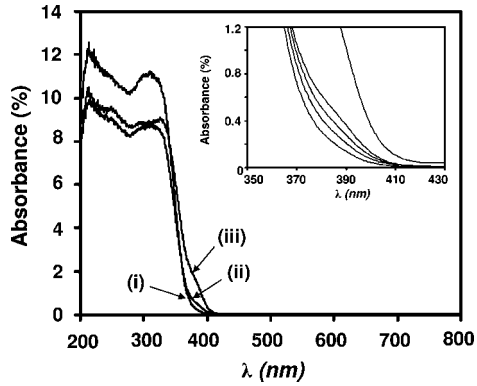

Figure 7. UV−vis DR absorption spectra obtained for mixed-phase nanocrystalline TiO_2 processed via sol−gel SMC. Rutile content varies as 0 (i), 40 (ii), and 60 (iii) wt%. In the inset, the spectra from left to right correspond to the rutile content of 5, 10, 20, 40, and 60 wt%, respectively.

primarily rutile-TiO_2, are first synthesized via sol−gel.[2,16] These two precursors are utilized for processing mixed-phase nanocrystalline TiO_2 with varying rutile content via SMC. It is observed that the photocatalytic activity of mixed-phase nanocrystalline TiO_2-processed via sol−gel SMC is a function of rutile content (Figure 9). The maximum photocatalytic activity (that is, maximum k_{app} and minimum normalized residual MB dye concentration) is observed at an optimum rutile content of 40 wt%, which suggests the significance of the synergistic effect between anatase-TiO_2 and rutile-TiO_2, which needs further attention. In order to explain the synergistic effect in detail, we present below a brief review of the literature where a similar observation has already been reported.

Review of the Literature Related to Synergistic Effect and Comparison of the Literature Data with the Present Data. A brief review of the literature reporting the synergistic effect has been summarized in Table 1.[4–13] It appears that in the literature, mixed-phase nanocrystalline TiO_2 has been processed via high temperature calcination treatment of amorphous-TiO_2 or anatase-TiO_2,[7,9,11,12] changing the pH,[4] the anion concentration,[8] or the precursor[10] during the processing, and physical mixing of the precursors[4,8] (similar to the sol−gel SMC as

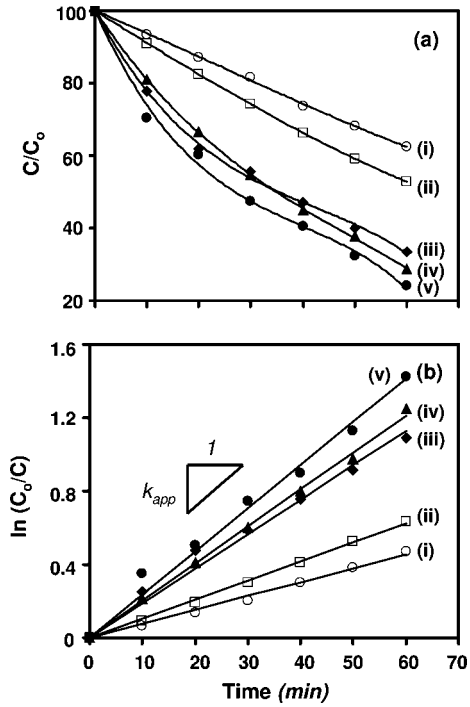

Figure 8. (a) Typical variation in the normalized residual MB dye concentration as a function of UV-exposure time, obtained for the two sol−gel-derived precursors, powder-B (i) and powder-A (ii), as well as for the mixed-phase nanocrystalline TiO_2 processed via sol−gel SMC with a rutile content of 0 (iii), 10 (iv), and 40 (v) wt%. (b) Typical plots, obtained using part a, for determining the k_{app}.

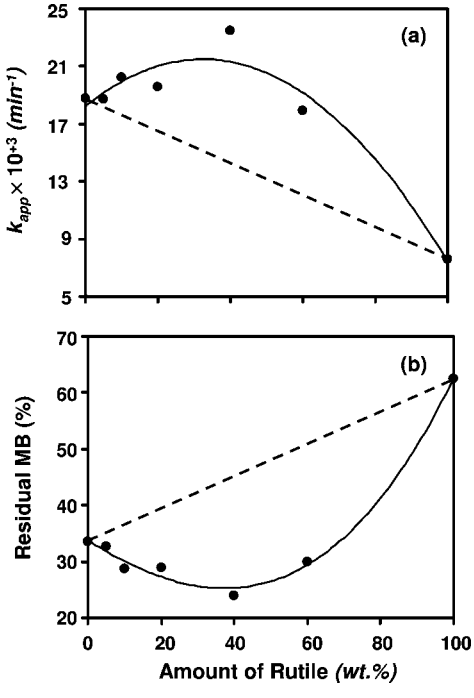

Figure 9. Variation in the k_{app} (a) and the normalized residual MB dye concentration corresponding to 60 min of UV-radiation exposure (b) as a function of the amount of rutile, obtained for mixed-phase nanocrystalline TiO_2-processed via sol−gel SMC. The dotted lines represent hypothetical variations in the absence of the synergistic effect between anatase-TiO_2 and rutile-TiO_2.

investigated here). Moreover, different investigators report different optimum rutile content corresponding to the maximum photocatalytic activity, which is noted to be within the range of 12−90 wt%. This range is relatively larger and may be attributed to the different conditions under which an optimum rutile content is obtained. Specifically, mixed-phase nanocrystalline TiO_2 with an optimum rutile content has been synthesized via different wet chemical techniques and tested for the photocatalytic activity with different catalytic agents. Moreover, these powders with an optimum rutile content have a broad range of specific surface area (9−113 $m^2 \cdot g^{-1}$). Hence, it appears that, because of the large number of involved variables having their respective values in a broader range, an optimum rutile content is possibly observed in a wider range. Nevertheless, the data presented in Table 1 does confirm the existence of an optimum amount of rutile in the mixed-phase nanocrystalline TiO_2 to obtain the maximum photocatalytic activity. Similar to these reports, in the present investigation, an optimum amount of rutile, corresponding to the maximum photocatalytic activity, has been observed for 40 wt% rutile content, which is well within the reported range.

In the literature, several physical parameters have been demonstrated to vary systematically as a function of rutile content in the mixed-phase nanocrystalline TiO_2. Since the photocatalytic activity is dependent on these parameters, it follows that in order to understand the dependence of the photocatalytic activity on the rutile content, it is necessary to know the variations in these parameters as a function of amount of rutile.

As shown in Figure 10a, the specific surface area of mixed-phase nanocrystalline TiO_2 has been demonstrated to decrease with increasing amount of rutile since the anatase-to-rutile phase transformation takes place in higher temperature range (>600 °C) and is accompanied by excessive grain growth.[4,7,17,18] Hence, with increasing rutile content, gradual decrease in the specific surface area has been observed. Since the specific surface area plays an important role in the surface adsorption of the dye molecules, the increasing rutile content should tend to reduce the photocatalytic activity of mixed-phase nanocrystalline TiO_2.

Moreover, the total pore volume and the average pore size have been reported to increase with increasing rutile content in mixed-phase nanocrystalline TiO_2, Figure 10b.[10] During the anatase-to-rutile phase transformation at higher temperatures, the increased grain-size distribution caused by the phase transformation introduces the mesopore structure with wider pore-size distribution and increased pore volume. These factors tend to increase the photocatalytic activity during the initial period of the phase transformation process. However, the excessive phase transformation at still higher temperatures leads to the loss of mesopore structure, which reduces the photocatalytic activity.

Apart from the specific surface area, the total pore volume and the average pore size, the band gap of mixed-phase nanocrystalline TiO_2 has also been demonstrated to be a function of rutile content.[8] As shown in Figure 10c, the band gap of mixed-phase nanocrystalline TiO_2 has been shown to decrease continuously with increasing amount of rutile since the band gap of pure anatase-TiO_2 (3.2 eV) is larger than that (3.0 eV) of pure rutile-TiO_2. This is confirmed in the present investigation as well by observing a systematic red shift in the absorption spectra with increasing rutile content (Figure 7). The e^-/h^+ recombination is known to be faster in rutile-TiO_2 due to its smaller and identical band gap for nanocrystallites of different sizes (as explained in detail in the following sections) and reduced electron mobility.[14] As a result, the photocatalytic activity of anatase-TiO_2 is invariably larger than that of rutile-TiO_2.[2] Hence, decreasing band gap with increasing rutile content

TABLE 1: A Brief Summary of the Literature Data Related to the Synergistic Effect As Reported for the Mixed-Phase Nanocrystalline TiO_2

optimum rutile (wt%)	synthesis method	anatase size (XRD) (nm)	rutile size (XRD) (nm)	BET surface area ($m^2 \cdot g^{-1}$)	catalytic agent	max. conversion (%) /max. k_{app} (min^{-1})	ref
12−15	sol−gel hydrothermal	12	35	85−87	hexane and methanol in air	25−45	4
15−20 (Brookite)	hydrothermal	20	30	78	phenol in water	94	5
	sol−gel under ultrasonic conditions	10	8	98	acetone in air	0.0053	6
23	precipitation	60	60	32	4-chlorophenol in water	0.02	7
26	microemulsion hydrothermal	13	12	113	methyl orange in water	0.0008	8
28	sol−gel (supercritical drying)	22	-	36	phenol in water	0.16	9
30	microemulsion hydrothermal (physical mixing)	-	-	-	methyl orange in water	0.0007	8
30	sol−gel hydrothermal	25[a]	50[a]	72	*p*-coumaric acid	-	10
40	sol−gel SMC	29	47	-	methylene blue in water	0.023	present investigation
42	vapor hydrolysis	38	46	27	phenol in water	50	11
52	sol−gel autocombustion	14	14	53	methylene blue in water	68	12
90	commercial	-	-	9	naphthalene in acetonitrile in water	0.8 $\mu M \cdot min^{-1}$	13

[a] Size estimated using HRTEM.

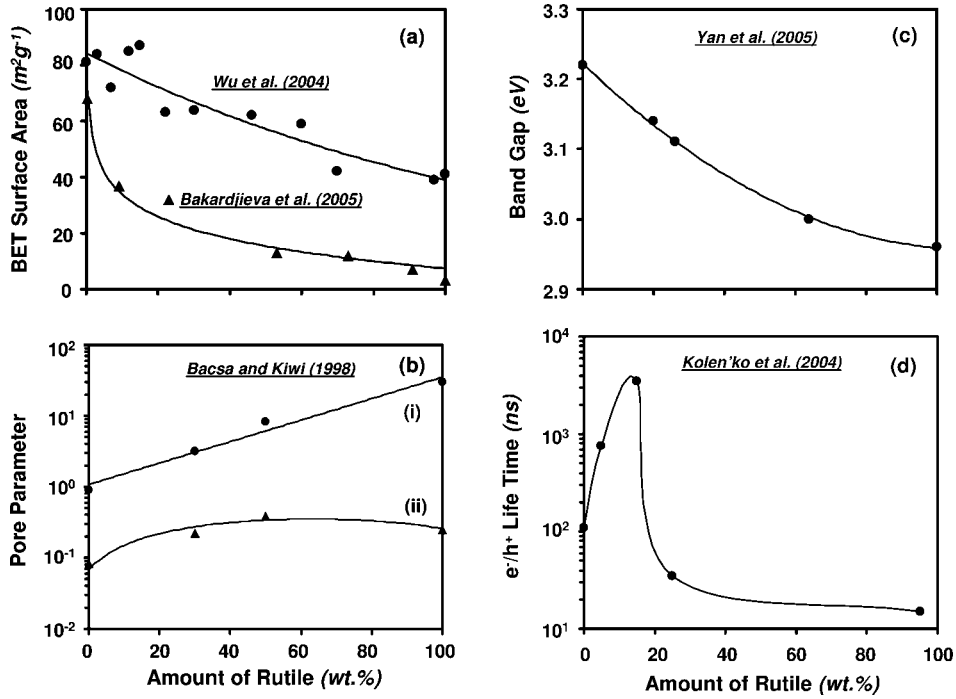

Figure 10. Literature data[4,5,7,8,10] showing the variation in different physical parameters of mixed-phase nanocrystalline TiO_2 as a function of amount of rutile. In part b, i and ii represent the average pore size (radius, nm) and the total pore volume ($cm^3 \cdot g^{-1}$).

would tend to reduce the photocatalytic activity of mixed-phase nanocrystalline TiO_2 (law-of-mixture).

Moreover, it has been demonstrated that (Figure 10d) the e^-/h^+ lifetime for mixed-phase nanocrystalline TiO_2 is dependent on the amount of rutile.[5] However, this variation appears to be quite different than that observed in Figures 10a−c. It is noted that the e^-/h^+ lifetime increases first with increasing amount of rutile and then decreases suddenly with further increase in rutile content. Hence, the increased e^-/h^+ lifetime would tend to increase the photocatalytic activity as the rutile content in the mixed-phase nanocrystalline TiO_2 increases. However, with further increase in the rutile content, the decreased e^-/h^+ lifetime would tend to reduce the photocatalytic activity of the mixed-phase nanocrystalline TiO_2.

Overall, from the literature data presented in Figure 10 it appears that as the rutile content in the mixed-phase nanocrystalline TiO_2 increases, the variation in the photocatalytic activity would be dependent on the variation in the specific surface area, the total pore volume and the average pore size, the band gap, and the e^-/h^+ lifetime. For smaller amount of rutile content, the decreasing specific surface area and the band gap would tend to reduce the photocatalytic activity of the mixed-phase nanocrystalline TiO_2. On the other hand, the enhanced pore volume, average pore-diameter, and the e^-/h^+ lifetime would tend to increase it.

If the photocatalytic activity of mixed-phase nanocrystalline TiO_2 processed via sol−gel SMC would have been dependent only on the specific surface area and the band gap, then the

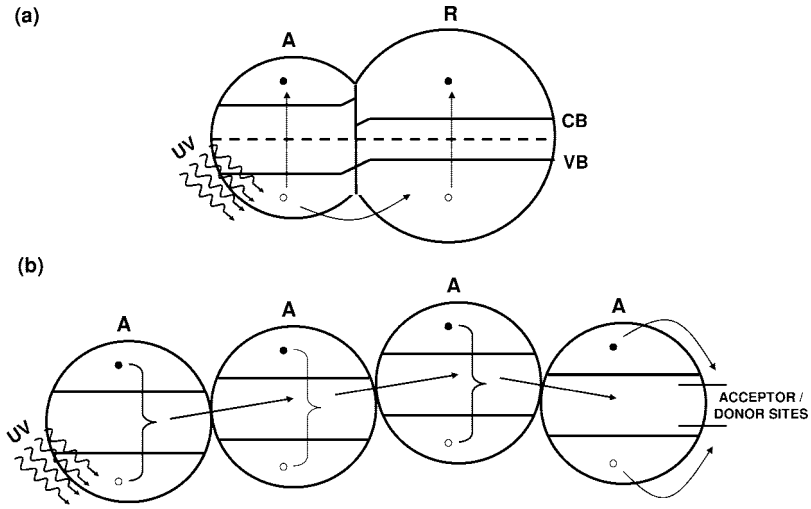

Figure 11. Schematic representation of the charge-separation mechanism (a) and the antenna mechanism (b) proposed in the literature for the enhanced e^-/h^+ lifetime in mixed-phase nanocrystalline TiO_2. A, R, CB, and VB represent anatase-TiO_2, rutile-TiO_2, the conduction band, and the valence band, respectively. In part b, the connected nanocrystallites are assumed to be of the same phase with the same crystallographic orientation.

photocatalytic activity would have followed the path as indicated by the dotted lines in Figure 9 (law-of-mixture). However, the experimentally observed variation in the photocatalytic activity significantly deviates from the dotted lines as noted from the drastic difference in the slopes of the graphs when the rutile content in the mixed-phase nanocrystalline TiO_2 begins to increase. Hence, it appears that the combined effect of the variation in the total pore volume, the average pore size, and the e^-/h^+ lifetime on the photocatalytic activity must be stronger than that of the variation in the specific surface area and the band gap. As a result, under these conditions, the photocatalytic activity of mixed-phase nanocrystalline TiO_2 must increase first with the addition of rutile-TiO_2 to anatase-TiO_2.

Further, the dotted lines in Figure 9 possibly suggest that these hypothetical variations may be dependent on the weighted average of the two phases involved (law-of-mixture). Hence, the deviation in the photocatalytic activity away from the dotted lines suggests the presence of strong electronic interaction between anatase-TiO_2 and rutile-TiO_2. Thus, a synergistic effect has been observed in the present investigation for mixed-phase nanocrystalline TiO_2 processed via sol−gel SMC. We believe that, among all the factors, the enhanced e^-/h^+ lifetime in the mixed-phase nanocrystalline TiO_2, Figure 10d, is possibly the major factor responsible for observing the synergistic effect in the present investigation.

Mechanisms Associated with Increased e^-/h^+ Lifetime for Mixed-Phase Nanocrystalline TiO_2. One of the proposed mechanisms, known as the "charge-separation mechanism",[14] associated with the increased e^-/h^+ lifetime for mixed-phase nanocrystalline TiO_2, is described schematically in Figure 11a. According to this mechanism, when anatase-TiO_2 and rutile-TiO_2 nanocrystallites are in contact with each other, the resulting band bending at the interface does not allow the electrons generated in anatase-TiO_2 to escape into rutile-TiO_2.[14,19] On the other hand, the same band bending allows the holes generated in anatase-TiO_2 to escape into rutile-TiO_2. This effectively separates the charges with the electrons accumulating in anatase-TiO_2 and the holes in rutile-TiO_2, which in turn enhances the e^-/h^+ lifetime, as demonstrated experimentally by others (Figure 10d).[5]

The second existing mechanism related to the increased e^-/h^+ lifetime, known as the "antenna mechanism" as proposed in the literature,[15] is presented in Figure 11b. This mechanism considers the connected anatase-TiO_2 nanocrystallites having the same lattice orientation. This allows the photoinduced e^-/h^+ pair to move via the multicrystallite transfer process, without recombination, from the site of their origin to nanocrystallite where the dye molecule is adsorbed. As a result, according to this mechanism, nanocrystallite in which the e^-/h^+ pair is created and nanocrystallite over which the dye molecule is adsorbed may be separated by a large distance. Thus, the entire chain of aligned nanocrystallites acts as an antenna to transfer the incoming photon energy from the light-absorption site to the reaction site. The charge separation ultimately takes place when the e^-/h^+ pair reaches the trap sites, thus leading to the increased e^-/h^+ lifetime.

Both of the proposed mechanisms are, however, associated with the major limitations. For example, it is well-known that nanocrystalline TiO_2 powder invariably contains a size distribution with a large half-width.[20,21] Second, the band gap of anatase-TiO_2 is dependent on nanocrystallite size;[21,22] and third, the anatase-to-rutile phase transformation is also dependent on nanocrystallite size.[2,17,18] Both of the existing mechanisms discussed above do not take these factors into consideration, and hence these mechanisms do not provide the complete description of the synergistic effect associated with the connected nanocrystallites of anatase-TiO_2 and ruitle-TiO_2 or with the connected nanocrystallites of anatase-TiO_2. As a result, the existence of optimum rutile content for observing the maximum photocatalytic activity in mixed-phase nanocrystalline TiO_2 cannot be predicted using these mechanisms.

To overcome these limitations associated with the existing mechanisms and to explain the reported variation in the e^-/h^+ lifetime as a function of amount of rutile, Figure 10d, we propose here a new model based on the band-gap variation in the connected nanocrystallites as a function of the size distribution and the phases involved. The "charge-separation mechanism" and the "antenna mechanism" are appropriately combined here in a single model.

Model Based on Band-Gap Variation in Connected Nanocrystallites as a Function of Size Distribution and Phases Involved. In Figure 12a, the connected nanocrystallites of pure anatase-TiO_2 (as proposed in the "antenna mechanism" but not necessarily having the same lattice orientation) with a

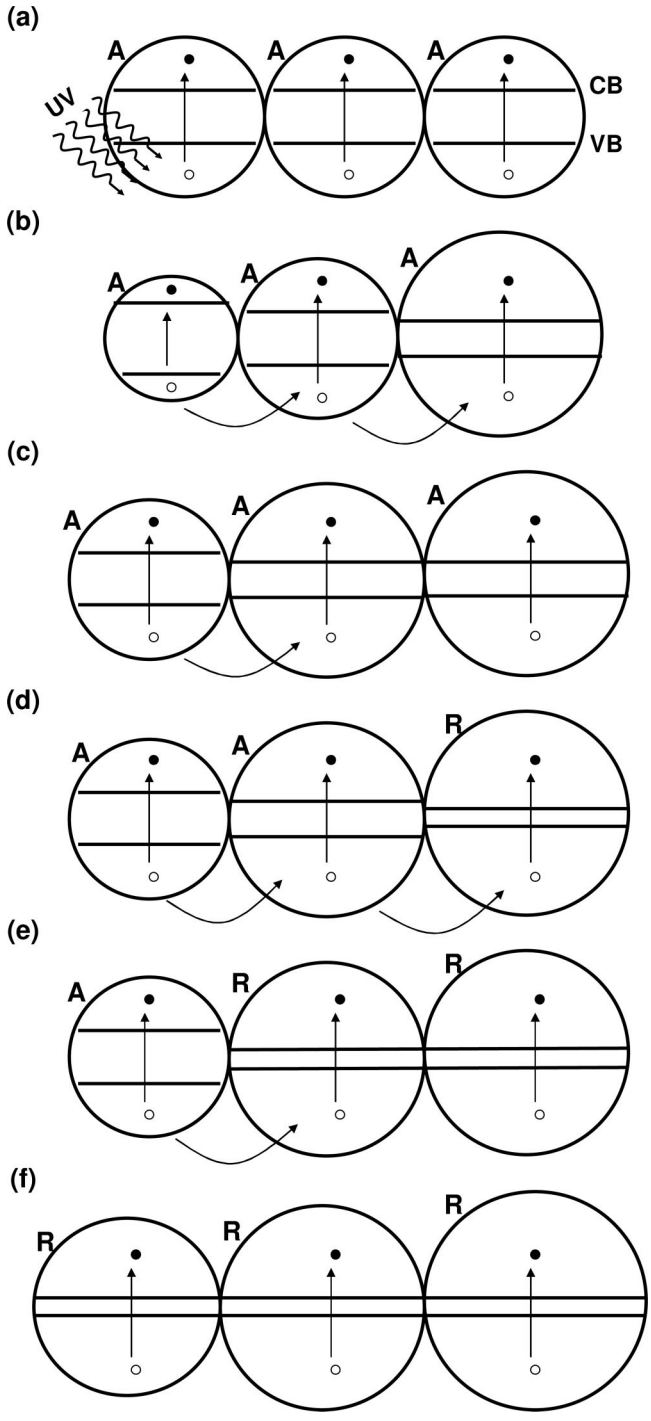

Figure 12. New model, proposed here, based on the bad-gap variation in the connected nanocrystallites as a function of the size distribution and the phases involved, which satisfactorily explains the existence of optimum rutile content in the mixed-phase nanocrystalline TiO_2 corresponding to the maximum photocatalytic activity. A, R, CB, and VB represent anatase-TiO_2, rutile-TiO_2, the conduction band, and the valence band, respectively.

monodispersed nanocrystallite size distribution, is schematically shown. Since the band gaps of these nanocrystallites would be the same due to their identical size, the driving force for the transfer of photoinduced hole from one nanocrystallite to the neighboring nanocrystallite would be minimum. As a result, the e^-/h^+ lifetime in anatase-TiO_2 with a monodispersed nanocrystallite size distribution would be very low leading to the reduced photocatalytic activity. The photocatalytic activity of pure anatase-TiO_2 with a monodispersed nanocrystallite size distribution has not been reported yet, which may be due to the issues associated with the processing such powders.

In practice, as mentioned earlier, anatase-TiO_2 synthesized via wet chemical routes contains a broad nanocrystallite size distribution with larger half-width (Figure 4) and the band gap of pure anatase-TiO_2 increases below a critical size. Hence, if the nanocrystallite size distribution is below this critical size, then the band gaps of the connected nanocrystallites would be different depending on their size, Figure 12b. As a result, the photoinduced hole produced in one nanocrystallite can easily escape into the other leading to the effective charge-separation (according to the "charge-separation mechanism" assuming that the mechanism is valid after replacing rutile-TiO_2 with anatase-TiO_2 (Figure 11a)). Due to the variation in the band gap, nanocrystallite located in the center acts as a sink as well as a source of holes, thus serving a dual function in this band-gap configuration. Hence, anatase-TiO_2 having a large fraction of such band-gap configuration of the connected nanocrystallites would have relatively longer e^-/h^+ lifetime leading to its higher photocatalytic activity. This also suggests the significance of nanocrystallite size distribution with larger half-width to achieve higher photocatalytic activity using anatase-TiO_2.

If a part of the nanocrystallite size distribution lies above the critical size, then that part of the size distribution would not exhibit the variation in the band gap as a function of size, Figure 12c. Under this circumstance, the transfer of holes from one nanocrystallite to the neighboring nanocrystallite would be restricted compared to that in the band-gap configuration shown Figure 12b. The present model assumes that nanocrystalline anatase-TiO_2 primarily contains a mixture of band-gap configurations of the connected nanocrystallites as shown in Figures 12b and 12c. The photocatalytic activity of pure anantase-TiO_2 would be then governed by the relative fractions of these band-gap configurations.

It is well-known that there also exists a critical size for the anatase-to-rutile phase transformation.[2,18] As a result of the existence of this critical size, the band-gap configuration in the connected nanocrystallites would be partially changed from that shown in Figure 12c to that shown in Figure 12d provided a part of the nanocrystallite size distribution crosses the critical size for the phase transformation. Hence, as a result of the increased rutile content (as normally observed during the calcination process or due to the addition of rutile-TiO_2 to anatase-TiO_2 (Figures 6a and 6b) with the strong electronic interaction in between them), the fraction of the band-gap configuration shown in Figure 12d would increase at the expense of that shown in Figure 12c. The mixed-phase nanocrystalline TiO_2 thus formed would now contain a mixture of band-gap configurations shown in Figures 12b−d. Although the phases involved are different, the band-gap configuration shown in Figure 12d appears to be similar to that shown in Figure 12b. In both the band-gap configurations, the nanocrystallite located in the center can serve a dual function. Hence, due to the change in the mixture of band-gap configurations in the connected nanocrystallites, the addition of rutile-TiO_2 would enhance the e^-/h^+ lifetime in the mixed-phase nanocrystalline TiO_2 relative to that in pure anatase-TiO_2. Hence, the present model suggests that, at the initial stage, the photocatalytic activity would tend to increase with increasing rutile content, which is in agreement with the experimental results obtained in this investigation (Figure 9).

However, with further increase in the amount of rutile-TiO_2, more number of contacts would be established in between rutile−rutile nanocrystallites having an identical band gap,

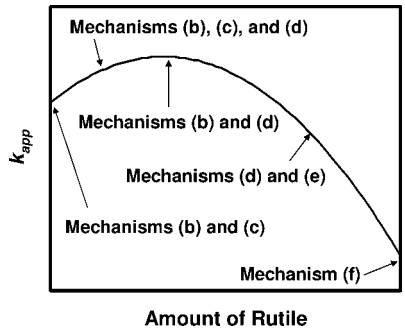

Figure 13. Schematic diagram showing the different mechanisms, as proposed in the new model (Figure 12), operating in the different regions of the graph of the variation in the k_{app} as a function of amount of rutile. The graph is an experimentally determined variation presented in Figure 9a.

Figure 12e. As mentioned earlier, rutile phase is normally formed as a result of the anatase-to-rutile phase transformation process, which occurs at higher temperatures (>600 °C), and this is invariably accompanied by the excessive growth in the nanocrystallite size of rutile-TiO_2. [4,7,17,18] Hence, in the present model, the nanocrystallite size distribution of rutile-TiO_2 is assumed to be well above the critical size required for the band-gap enhancement, which is strongly supported by the present XRD and TEM data. Under this assumption, in Figure 12e (and also in Figure 12f), nanocrystallites of rutile-TiO_2 of different sizes having identical band gaps are considered. As the fraction of such band-gap configuration increases, the e^-/h^+ lifetime would be reduced, which in turn would tend to decrease the photocatalytic activity of the mixed-phase nanocrystalline TiO_2. Hence, it appears that the maximum photocatalytic activity would be obtained for an optimum rutile content in the mixed-phase nanocrystalline TiO_2. Above this optimum value, the effect of the band-gap configuration shown in Figure 12e would be more pronounced than that of the band-gap configuration shown in Figure 12d due to the variation in their relative fractions. Hence, increasing the rutile content, above an optimum value, would decrease both the e^-/h^+ lifetime and the photocatalytic activity of the mixed-phase nanocrystalline TiO_2. According to the present model, mixed-phase nanocrystalline TiO_2 with an optimum rutile content would ideally contain a mixture of band-gap configurations shown in Figures 12b and 12d.

For pure rutile-TiO_2, Figure 12f, the band gap would not change from one nanocrystallite to the other as their size, although different, would be well above the critical size required for the band-gap variation (Figure 5). This may drastically reduce the e^-/h^+ lifetime for pure rutile-TiO_2, as experimentally demonstrated by others,[5] which in turn would significantly reduce its photocatalytic activity (Figure 9). Smaller specific surface area of pure rutile-TiO_2 would be another contributing factor for its lowest photocatalytic activity.

Thus, the present model suggests that the maximum photocatalytic activity would be obtained for mixed-phase nanocrystalline TiO_2 having an optimum rutile content. The various mechanisms discussed above, based on the band-gap variation in the connected nanocrystallites as a function of the size distribution and the phases involved, operate for different rutile contents and have been summarized in Figure 13, which is an experimentally observed variation in the k_{app} as a function of amount of rutile (Figure 9a). Thus, the new model proposed here satisfactorily explains the existence of optimum rutile content in the mixed-phase nanocrystalline TiO_2, for observing the maximum photocatalytic activity, by overcoming the limitations of the models proposed earlier in the literature. As seen from Figure 12, the model predicts that the band gap of mixed-phase nanocrystalline TiO_2 should decrease with increasing rutile content, which has been experimentally confirmed in the present investigation (Figure 7) by observing a systematic red shift in the absorption spectra with increasing rutile content. We believe that the present model is valid irrespective of the processing method used for obtaining mixed-phase nanocrystalline TiO_2 with varying rutile content.

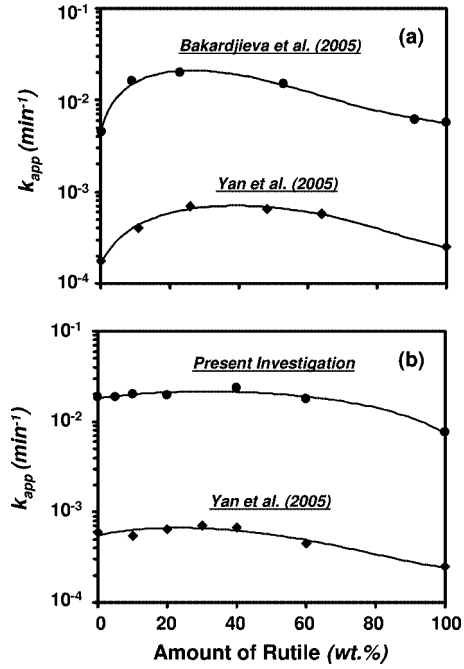

Figure 14. Comparison of the synergistic effect (in the half-logarithmic scale) observed for mixed-phase nanocrystalline TiO_2 with varying rutile content, processed via high temperature calcination treatment[7] (a) and controlling the anion concentration[8] (a), with that observed for mixed-phase nanocrystalline TiO_2 processed via physical mixing[8] (b) and the sol−gel SMC (present investigation) (b) techniques.

Comparison of Synergistic Effect in Mixed-Phase Nanocrystalline TiO_2 Obtained via Different Processing Techniques. In Figure 14, which is plotted in the half-logarithmic scale, we compare the nature of the variation in the k_{app} as a function of amount of rutile as reported for the mixed-phase nanocrystalline TiO_2 obtained via high temperature calcination treatment[7] and controlling the anion concentration,[8] (Figure 14a) with that reported for the mixed-phase nanocrystalline TiO_2 obtained via physical mixing[8] and sol−gel SMC (present investigation) methods (Figure 14b). The comparison in the half-logarithmic scale shows that the incorporation of rutile-TiO_2 into anatase-TiO_2 results in better improvement in the photocatalytic activity of mixed-phase nanocrystalline TiO_2 obtained via high temperature calcination treatment and controlling the anion concentration (Figure 14a) than that obtained using the physical mixing and the sol−gel SMC techniques (Figure 14b). As shown in Figures 6c and 6d, the sol−gel SMC process, which is based on the solvent mixing of the sol−gel-derived precursors followed by the drying and calcination treatments, possibly results in mixed-phase nanocrystalline TiO_2, which contains some domains of anatase-TiO_2 and rutile-TiO_2, which are not electronically coupled with each other. As a result, it appears that the synergistic effect is relatively more apparent in mixed-phase nanocrystalline TiO_2 obtained via other techniques (Figure 14a). Nevertheless, in the present investigation, the synergistic effect has certainly been confirmed for the mixed-phase nanoc-

rystalline TiO_2 obtained via sol−gel SMC with an optimum rutile content of 40 wt%.

Conclusions

Mixed-phase nanocrystalline TiO_2 with varying rutile content has been synthesized using the sol−gel SMC. The photocatalytic activity of mixed-phase nanocrystalline TiO_2 has been observed to be a function of the amount of rutile, with an optimum rutile content of 40 wt%, which is in agreement with the reported literature. The existence of an optimum rutile content suggests the synergistic effect between anatase-TiO_2 and rutile-TiO_2, which has been satisfactorily explained using a new model based on the band-gap variation in the connected nanocrystallites as a function of the size distribution and the phases involved. The present model overcomes the limitations of the existing models proposed earlier in the literature.

Acknowledgment. Authors thank the Department of Science and Technology (DST), India (Project # GAP 205139), and the Council of Scientific and Industrial Research (CSIR), India (Network Project # NWP0010 and Task Force Project # CMM0019), for funding the ceramic, nanotechnology, and photocatalysis research at NIIST. Authors also thank Mr. M. R. Chandran, Mr. P. Mukundan (both from NIIST-CSIR, India), and Mr. Narendra (Icon Analytical, India) for conducting the SEM, FTIR, and HRTEM analyses, respectively.

References and Notes

(1) Fujishima, A.; Rao, T. N.; Tryk, D. A. *J. Photochem. Photobiol. C* **2000**, *1*, 1.
(2) Baiju, K. V.; Shukla, S.; Sandhya, K. S.; James, J.; Warrier, K. G. K. *J. Phys. Chem. C* **2007**, *111*, 7612.
(3) Zhang, Z.; Wang, C.-C.; Zakaria, R.; Ying, J. Y. *J. Phys. Chem. B* **1998**, *102*, 10871.
(4) Wu, C.; Yue, Y.; Deng, X.; Hua, W.; Gao, Z. *Catal. Today* **2004**, *93−95*, 863.
(5) Kolen'ko, Y. V.; Churagulov, B. R.; Kunst, M.; Mazerolles, L.; Justin, C. C. *Appl. Catal., B* **2004**, *54*, 51–58.
(6) Yu, J. C.; Yu, J.; Ho, W.; Zhang, L. *Chem. Commun.* **2001**, *19*, 1942.
(7) Bakardjieva, S.; Subrt, J.; Stengl, V.; Dianez, M. J.; Sayagues, M. J. *Appl. Catal., B* **2005**, *58*, 193.
(8) Yan, M.; Chen, F.; Zhang, J.; Anpo, M. *J. Phys. Chem. B* **2005**, *109*, 8673.
(9) Chen, L.; Zhu, J.; Liu, Y.-M.; Cao, Y.; Li, H.-X.; He, H.-Y.; Dai, W.-L.; Fan, K.-N. *J. Mol. Catal.* **2006**, *255*, 260.
(10) Bacsa, R. R.; Kiwi, J. *Appl. Catal., B* **1998**, *16*, 19.
(11) Chan, C. K.; Porter, J. F.; Li, Y.-G.; Guo, W.; Chan, C.-M. *J. Am. Ceram. Soc.* **1999**, *82*, 566.
(12) Xiao, Q.; Si, Z.; Yu, Z.; Qiu, G. *Mater. Sci. Eng.* **2007**, *137*, 189.
(13) Ohno, T.; Tokieda, K.; Higashida, S.; Matsumura, M. *Appl. Catal. A.* **2003**, *244*, 383.
(14) Sun, B.; Vorontsov, A. V.; Smirniotis, G. *Langmuir* **2003**, *19*, 3151.
(15) Wang, C.-Y.; Pagel, R.; Dohrmann, J. K.; Bahnemann, D. W. *C. R. Chim.* **2006**, *9*, 761.
(16) Baiju, K. V.; Shukla, S.; Sandhya, K. S.; James, J.; Warrier, K. G. K. *J. Sol-Gel Sci. Technol.* **2008**, *45*, 165.
(17) Kumar, K.-N. P.; Fray, D. J.; Nair, J.; Mizukami, F.; Okubo, T. *Scr. Mater.* **2007**, *57*, 771.
(18) Zang, H.; Banfield, J. F. *J. Mater. Res.* **2000**, *15*, 437.
(19) Henisch, H. K. *Semiconductor contacts: an approach to ideas and models*; Oxford University Press: New York, 1984.
(20) Venktatachalam, N.; Palanichamy, M.; Murugesan, V. *Mater. Chem. Phys.* **2007**, *104*, 454.
(21) Lin, H.; Huang, C. P.; Li, W.; Ni, C.; Shah, S. I.; Tseng, Y.-H. *Appl. Catal. B.* **2006**, *68*, 1.
(22) Ding, Z.; Lu, G. Q.; Greenfield, P. F. *J. Phys. Chem. B* **2004**, *104*, 4815.

JP712174Y